Extinction in Non-Premixed Ethanol Spray Flames Using Direct Numerical Simulation

Joshua C.K. Tang, Haiou Wang, Evatt R. Hawkes
University of New South Wales, Sydney, Australia
Michele Bolla
ETH Zurich, Zurich, Switzerland

1 Introduction

Flame extinction is an important phenomenon to consider when designing combustion devices with high levels of turbulence. In general, high turbulence increases the flame surface area and the rate of diffusive mixing, allowing for smaller combustion chambers and higher heat release rates. However, if mixing rates exceed chemical reaction rates, heat and important radicals can be transported away from the reaction zone resulting in local extinction [1]. The result of local extinction is the production of "flame holes", which potentially allow unburned fuel to escape, increasing hydrocarbon emissions as well as decreasing combustion efficiency. If extinction rates are high enough, flame instabilities or even global extinction can occur, an undesirable situation for any combustion system. While gaseous flame extinction is already complex, the introduction of liquid fuel creates additional difficulties. As a result extinctions in spray flames have not been studied in the same detail as those in gaseous flames. An improved understanding of spray flame extinction is of prime importance to optimise performance of practical combustion devices and develop predictive spray combustion models.

Direct numerical simulation (DNS) presents a viable approach to understand the microscopic details of extinction as it provides high temporal and spatial resolutions to fully capture the flow field as well as the scalar structures. DNS has been successfully applied in numerous single phase studies of extinction [1–4]. It has been found that scalar dissipation rate is a controlling parameter in the flame extinction process. However, it is not clear how the scenario looks like in spray flames.

In the above context, DNS of temporally evolving, non-premixed planar ethanol spray flames, which feature different levels of extinction, are performed. The configuration and flow parameters are broadly based on previous gas phase non-premixed flame studies, in which there are strong interactions between the shear-driven turbulence and chemistry [3, 4]. In the DNS, the Stokes number is varied between each simulation while the liquid mass loading, Reynolds and Damköhler numbers are kept constant. It is expected that, in the current study of spray flames, the Stokes number substantially influences the flow dynamics and the extinction characteristics of the flame.

Correspondence to: joshua.tang@unsw.edu.au   1

2 Configuration and Numerical Methods

The chosen configuration features temporally evolving, planar jet spray flames. This configuration is attractive as it maximises the interaction between droplet, turbulence and flame with reasonable computational costs. Ethanol was chosen as the fuel, as it is a relatively simple fuel which is liquid at atmospheric pressure. In addition, it has commercial applications and may be seen as an attractive petroleum substitute. The parameters were selected to maximise Re while still considering multiphase physics and detailed chemical kinetics. The fuel stream consists of 40% C_2H_5OH and 60% N_2 by volume. The surrounding oxidiser streams consist of 33% O_2 and 67% N_2. This composition was chosen to increase the extinction scalar dissipation rate (χ_q) of the flame to $\chi_q = 2600$ 1/s. This χ_q was chosen so that global extinction did not occur in the simulation. The initial temperature of both streams is set to 550 K to make the flame more resistant to extinction and pressure is set to atmospheric.

The streamwise velocity is $\Delta U/2$ in the central fuel stream, and $-\Delta U/2$ in the surrounding oxidizer streams, where $\Delta U = 288$ m/s. The jet height (H) is set to 0.96 mm. The Reynolds number of the jet is denoted by $Re_{jet} = \Delta U H/\nu_f$, where ν_f is the kinematic viscosity of the pure fuel stream. In the present work $Re_{jet} = 6000$. The initial velocity shear layer thickness, δ_u, is $H/5$, and the initial thickness of the mixture fraction variation, δ_Z, is 0.483 mm. The initial width of the fuel slab is denoted by $H_Z = H + \delta_Z - \delta_u$, and is greater than H to ensure that initially the mixture fraction (Z) approaches unity in the centre of the jet. Initial profiles of velocity and mixture fraction are specified using tanh-based profiles. In order to trigger shear generated turbulence, the mean velocity field is perturbed by homogeneous isotropic turbulence. This isotropic turbulence is filtered outside of the jet. The initial integral length scale, l_t, is H/3, and the initial turbulence intensity, u', is $0.05\Delta U$. Combustion is initialised with a steady laminar flamelet solution at an initial scalar dissipation rate, $\chi = 0.75\chi_q$, where χ_q is the quenching scalar dissipation rate obtained based on the initial conditions from the DNS. The jet Damköhler number, $Da = \chi_q t_j = 0.008$, where t_j is the transient jet time, defined as $t_j = H/\Delta U$. This Damköhler number is sufficiently low to induce local extinction. The domain size is $L_x = 8H$ in the stream-wise direction (x), $L_y = 14H$ in the transverse direction (y), and $L_z = 6H$ in the span-wise direction (z).

Fuel is supplied as both liquid (75% by mass) and gas. The gaseous fuel is needed in order to stabilise the initial flame when the droplets undergo evaporation. The spray is monodisperse, and the droplet diameter (D) is determined from the target Stokes number. The Stokes number is defined as $St = \tau_p/t_j$, where τ_p is the particle relaxation time defined as $\tau_p = \rho_d D^2/18\mu$. Two DNS cases with different Stokes numbers of 2.5 and 20 are studied in this work, which corresponds to droplet diameters of 2.3 and 6.5 μm, respectively. The St = 2.5 case has a short evaporation time, with complete evaporation occurring by 10 t_j, and is similar to gas phase combustion after this time. The St = 20 case has a substantially larger evaporation time with complete evaporation occurring after 50 t_j, allowing for flame-droplet interactions to occur. The initial droplet temperature is 300 K.

The governing equations are solved using the DNS code, S3D. The spatial derivatives are approximated using an 8th order central difference scheme [6] and time advancement is handled using a low-storage, 4th order Runge-Kutta method [7]. The liquid phase is treated using a Lagrangian particle tracking method using the same droplet equations as Borghesi *et al.* [8] but with ethanol fuel properties. The liquid and gas phase are two-way coupled, where gas phase properties are interpolated to the droplet locations using a 4th order Lagrangian interpolation scheme and droplet source terms are distributed linearly to the eight nearest Eulerian nodes [9].

The chemical kinetic mechanism is a reduced, 28 species ethanol mechanism featuring dynamic stiffness re-

moval [10]. This mechanism was developed from a detailed mechanism developed by Mittal *et al.* [11]. This mechanism was validated by Bhagatwala *et al.* [10] at atmospheric pressure and showed good agreement with the detailed mechanism.

The grid resolution required to resolve the Kolmogorov length scale, η_k, was inferred from past well resolved DNS studies which feature similar slot jet configurations [3, 5]. Following the recommendations of references [3,5] a grid size no larger than twice the size of the Kolmogorov is sufficient to resolve the turbulence. In this case, the Kolmogorov length scale is approximately 9.7 μm at the start of the simulation. Thus the grid resolution is $\Delta x = 17$ μm, which is uniform throughout the domain. This results in 0.57 grid points across the Kolmogorov scale. Since the turbulence length scales grow in time, at 20 t_j, the Kolmogorov length scale is 13 μm and there are 0.73 grid points across the Kolmogorov length scale. Comparison of the DNS cases with those run at half-resolution was also carried out, and it showed good agreement between the DNS and half-resolved cases for the mean and root mean square (RMS) values of different variables. Qualitative trends presented in this paper were also observed in the half-resolved cases.

3 Results

Figure 1 shows the instantaneous contours of temperature overlaid with the stoichiometric contour, taken at the central z-plane at 30 t_j. This time coincides with approximately the maximum extinction for the St = 20 case. The droplets in the St = 2.5 cases have fully evaporated, while the St = 20 case has approximately 30% of the liquid fuel remaining. The figures show a highly contorted stoichiometric surface with regions of burning and extinguished flame zones. It is noted that the St = 20 case has a small proportion of its remaining droplets moving from the fuel-rich jet through the higher temperature, reactive, stoichiometric region and into the fuel-lean region.
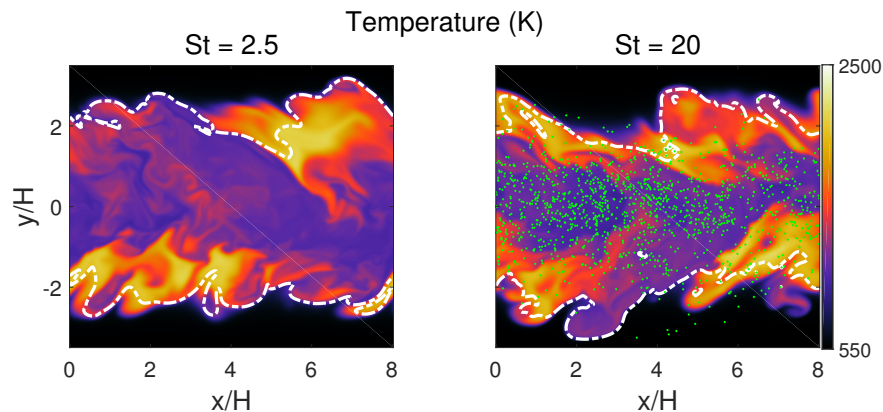

Figure 1: Instantaneous temperature at 30 t_j for St = 2.5 and St = 20. White dashed line represents the stoichiometric mixture fraction isoline; green dots represent droplet positions.

To quantify the level of extinction, the area of burning stoichiometric isosurface is compared against the total area of the stoichiometric isosurface. A region is considered burning if the OH mass fraction is greater than 50% of the laminar extinction value, $Y_{OH} = 0.0016$. The time variation of the fraction of burning surface area according to this definition for the two cases is presented in figure 2 (left). It is seen that the St = 20 case exhibits substantially higher extinction, with a maximum extinction of approximately 50%. In addition, the St = 20 case extinguishes much more rapidly compared to the St = 2.5 case, reaching the

maximum extinction approximately 10 t_j earlier. Considering the mean stoichiometric scalar dissipation rate in figure 2 (right) it shows that the St = 2.5 case exhibits much higher scalar dissipation rates during the extinction phase (20 - 40 t_j) however the extinction during this period is significantly smaller compared to the St = 20 case. This shows that the scalar dissipation rate is not the only factor which controls the extinction in the presented spray flames.
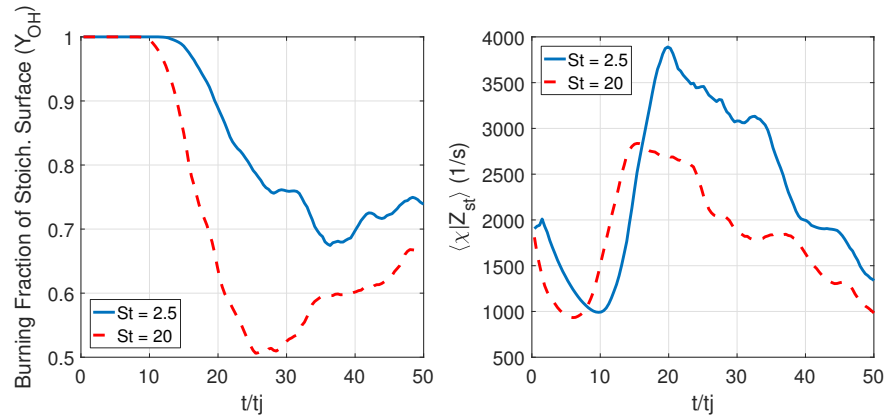

Figure 2: Temporal evolution of extent of extinction (left). Evaluated as the fraction of the stoichiometric surface with Y_{OH} values greater than 50% of the steady laminar extinction value. Temporal evolution of mean scalar dissipation conditioned on stoichiometric mixture fraction (right).

The increased level of extinction in the St = 20 case is a result of the large inertia and long evaporation time allowing the droplets to penetrate the reaction zone. Once in the reaction zone, evaporative cooling results in a loss of energy from the reaction zone thus weakening the flame. Figure 3 shows temporal evolution of the surface-integral of the droplet energy sink term (S_e), which represents the energy required for droplet evaporation and heating, along the stoichiometric mixture fraction isosurface compared to the surface integral of the heat release over the same surface. The total energy source term is roughly 4% of the heat release for the St = 20 case. This contribution is consistent for the majority of the simulation time, from 10 t_j to 35 t_j. In contrast, the St = 2.5 case does not show any interaction at any time during the simulation.
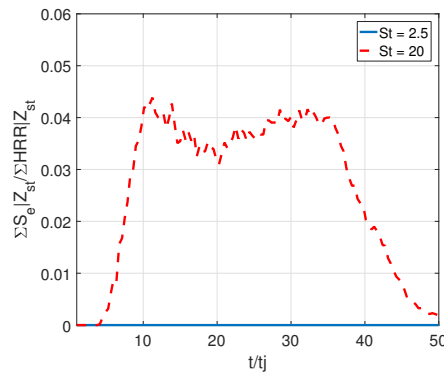

Figure 3: Temporal evolution of droplet energy sink term and heat release conditioned on stoichiometric isosurface.

Next, the chemical effects on the flame extinction are explored. An additional contributor to the increased extinction in the St = 20 case may be the deposition of fuel at the reaction zone due to evaporation, resulting

in radical depletion due to fuel-radical reactions. The reduction in OH reduces the overall heat release as its reaction with CO and H_2 contributes to a large percentage of heat release in most hydrocarbon flames [12]. Figure 4 presents the mean reaction rates for the major OH consumption pathways, as well as the total OH consumption rate, conditioned on the distance (L) from the stoichiometric isosurface in the two DNS cases at 5 and 10 t_j. The local distance from the stoichiometric surface is computed by solving the Eikonal equation, $|\nabla L| = 0$. Note that negative distances represent the oxidiser stream side while positive distances represent the fuel stream side. As expected, reactions of OH with CO and H_2 consumes most of the OH for both cases at both times. Reactions of OH with C_2H_5OH are approximately zero at the stoichiometric surface at 5 t_j for both cases. However, at 10 t_j droplets in the St = 20 case have moved into the reaction zone, and as a result reactions of OH with the C_2H_5OH molecule become significant. This set of reactions constitutes the third largest consumption pathway for the OH radical. In addition, the reaction rates of fuel fragment reactions (CH_2O, C_2H_4, HCO) also increase for the St = 20 case, as a result of the higher availability of fuel at the reaction zone. These reactions influence the flame extinction behaviour significantly as they do not produce additional radicals like H or OH which are required to sustain the flame. It is also observed, in the St = 20 case, the CO reaction is reduced relative to that in the St = 2.5 case. The presence of fuel fragments reduces the reaction rate of CO, as fuel fragment molecules exhibit greater reactivity with OH compared with CO [13]. The total consumption of OH in the St = 20 case is increased by 30% compared to the St = 2.5 case, due to the increased reaction rates of OH with fuel and fuel fragments. This results in a net reduction of OH, promoting extinction in the St = 20 case.
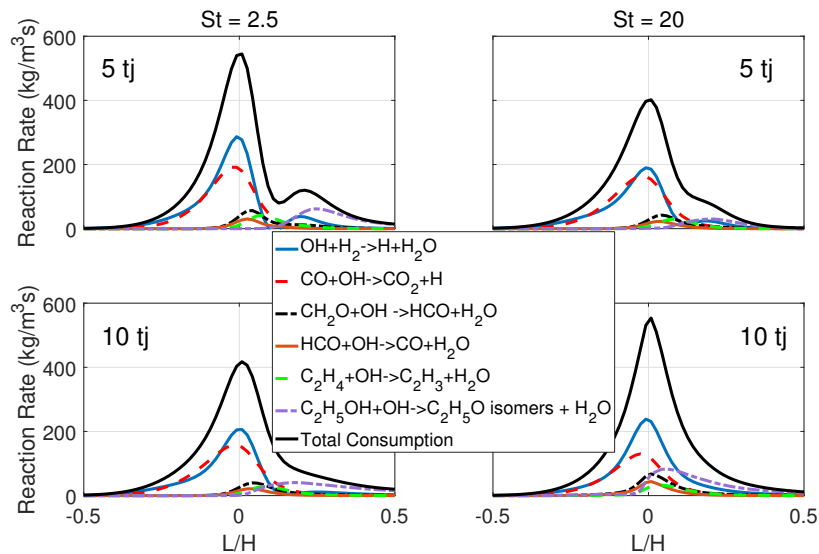

Figure 4: Mean reaction rates for major consumption pathways for OH radical. Solid black line represents the total consumption of OH

4 Conclusions

Extinction in non-premixed ethanol spray flames has been studied using direct numerical simulations. Greater extinction in the St = 20 case is a result of droplets entering the reaction zone and evaporating, resulting in extinction due to a combination of evaporative cooling and chemical kinetic effects. Evaporative cooling weakens the flame by absorbing energy released by the chemical reactions, while the chemical

effects are due to fuel vapour produced by evaporation reducing the concentration of important radicals, like OH, in the reaction zone. Both of these effects weaken the flame, making it more sensitive to the effects of turbulent straining (in the form of scalar dissipation rate).

References

[1] C. Pantano. (2004). Direct simulation of non-premixed flame extinction in a methane-air jet with reduced chemistry. J. Fluid Mech. 514: 231.

[2] P. Sripakagorn, S. Mitarai, G. Kosály, and H. Pitsch. (2004). Extinction and reignition in a diffusion flame: a direct numerical simulation study. J. of Fluid Mech. 518: 231.

[3] E. R. Hawkes, R. Sankaran, J. C. Sutherland, and J. H. Chen. (2007). Scalar mixing in direct numerical simulations of temporally evolving plane jet flames with skeletal CO/H2 kinetics. Proc. Combust. Inst. 31: 1633.

[4] D. Lignell, J. Chen, and H. Schmutz. (2011). Effect of Damköhler number on extinction and reignition in non premixed flames using DNS. Combust. Flame. 158: 949.

[5] C. S. Yoo, E. S. Richardson, R. Sankaran, and J. H. Chen. (2011). A DNS study on the stabilization mechanism of a turbulent lifted ethylene jet flame in highly-heated coflow. Proc. Combust. Inst. 33: 1619.

[6] J. H. Chen, A. Choudhary, B. de Supinski, M. DeVries, E. R. Hawkes, S. Klasky, W. K. Liao, K. L. Ma, J. Mellor-Crummey, N. Podhorszki, R. Sankaran, S. Shende and C. S. Yoo. (2009). Terascale direct numerical simulations of turbulent combustion using S3D. Computational Science & Discovery. 2:1.

[7] C. A. Kennedy and M. H. Carpenter. (1994). Several new numerical methods for compressible shear-layer simulations. Applied Numerical Math. 14: 397.

[8] G. Borghesi, E. Mastorakos, and R. Cant. (2013). Complex chemistry DNS of n-heptane spray autoignition at high pressure and intermediate temperature conditions. Combust. Flame. 157:1254 – 1275.

[9] A. Neophytou, E. Mastorakos, and R. Cant. (2010) DNS of spark ignition and edge flame propagation in turbulent droplet-laden mixing layers. Combust. Flame. 157:1071.

[10] A. Bhagatwala, J. H. Chen, and T. Lu. (2014). Direct numerical simulations of hcci/saci with ethanol. Combust. Flame. 161: 1826.

[11] G. Mittal, S. M. Burke, V. A. Davies, B. Parajuli, W. K. Metcalfe, and H. J. Curran. (2014). Autoignition of ethanol in a rapid compression machine. Combust. Flame. 161: 1164.

[12] S. Dooley, M. Uddi, S. H. Won, F. L. Dryer and Y. Ju. (2012). Methyl butanoate inhibition of n-heptane diffusion flames through an evaluation of transport and chemical kinetics. Combust. Flame. 159: 1371.

[13] K. K. Kuo. (2005). Principles of Combustion. John Wiley & Sons Incorporated. New Jersey, USA.